Hindawi
Journal of Renewable Energy
Volume 2020, Article ID 1907530, 10 pages
https://doi.org/10.1155/2020/1907530

Research Article

A Computationally Efficient Multidiode Model for Optimizing the Front Grid of Multijunction Solar Cells under Concentration

Chris H. van de Stadt,[1,2] Pilar Espinet Gonzalez,[2] Harry A. Atwater,[2] and Rebecca Saive[1]

[1]*Mesa+ Institute for Nanotechnology, University of Twente, Enschede 7522 NB, Netherlands*
[2]*Thomas J. Watson Laboratories of Applied Physics and Material Science, California Institute of Technology, Pasadena, CA 91125, USA*

Correspondence should be addressed to Rebecca Saive; r.saive@utwente.nl

Received 10 February 2020; Revised 25 June 2020; Accepted 30 June 2020; Published 16 July 2020

Academic Editor: Jayanta Mondol

We have developed a computationally efficient simulation model for the optimization of redirecting electrical front contacts for multijunction solar cells under concentration, and we present its validation by comparison with experimental literature results. The model allows for fast determination of the maximum achievable efficiency under a wide range of operating conditions and design parameters such as the contact finger redirecting capability, period and width of the fingers, the light concentration, and the metal and emitter sheet resistivity. At the example of a state-of-the-art four-junction concentrator solar cell, we apply our model to determine ideal operating conditions for front contacts with different light redirection capabilities. We find a 7% relative efficiency increase when enhancing the redirecting capabilities from 0% to 100%.

1. Introduction

Shading, parasitic absorption, and resistivity of the electrical front contacts constitute the largest individual loss mechanism in many solar cells [1]. On one hand, the front side needs to transmit as much light as possible in order to maximize the short circuit current. On the other hand, it has to be electrically conductive in order to minimize resistive losses. Due to the optoelectronic properties of solids, good electron conductors are generally bad light transmitters and vice versa. This leaves us with a delicate trade-off between transmission and conduction in designing the sun-facing side of a solar cell.

In most types of solar cells, for example, standard multijunction (MJ) solar cells, this trade-off is settled by applying a metal grid to the front side of the cell. The various design parameters such as the spacing between the grid lines and the width of the lines are then optimized for a compromise between low shading and low resistivity (see, for example, [2]). For a more accurate optimization, the absorption of a specific incoming light spectrum is determined by means of ray-tracing and wave-optical algorithms, and those results are fed into device simulations such as the simulation program with integrated circuit emphasis (SPICE) [3, 4] model.

In concentrator applications, the incoming light is concentrated onto a small area to increase efficiency and decrease material costs. Due to the enhanced Fermi level splitting under concentration, the open circuit voltage increases with the logarithm of the concentration. The short circuit current density increases proportionally to the concentration which simultaneously increases resistive power losses. Hence, maintaining a high fill factor with increased concentration requires the use of lower resistivity contacts. Due to this trade-off, the optimal operating point at which the efficiency is maximum can only be determined by considering resistivity, shading, and concentration simultaneously [4].

One way to improve the front grid conductivity without inducing additional shading is to increase the cross section of the contact without increasing the width, so by fabrication of large height-to-width ratio contacts, also referred to as

high aspect ratio contacts. The fabrication of high aspect ratio contacts has been demonstrated by evaporation [5], electroplating [6], printing [7–10], and embedding [11]. Further performance improvement can be achieved with contacts that do not reflect all the incoming light away from the cell but instead redirect part of the incoming light towards the active cell area. Examples include trapezoidal electroplated contacts [6], catoptric electrodes [12], and effectively transparent contacts (ETCs) [7, 8, 10, 13, 14]. This further increases the cell's efficiency by allowing more photons to be absorbed, thus increasing the short circuit current for a given grid coverage. However, as the fraction of the light being redirected to the cell for a certain geometry is often not precisely known, this additional degree of freedom in the design creates an extra variable to be taken into account in modeling such cells.

Running extensive optical and semiconductor models over such a vast parameter space becomes computationally expensive, creating the need for a computationally efficient model for optimizing partially redirecting front grids for MJ solar cells under concentration. The goal of this study was to find an easy-to-use, computationally inexpensive, and yet accurate model for front grid optimization of concentrator MJ solar cells.

There are a wide variety of approaches for modeling the electrical performance of MJ solar cells under concentration depending on the modeler's main goal. The single-diode model is the simplest of them and is in some cases sufficient for a rough estimate of the cell's behavior [15, 16]. However, it fails to take into account the effects of distributed resistances, the individual subcell's characteristics, and current mismatching between the subcells. Therefore, a single-diode model is unable to cope with changes on the subcell level and is unreliable when a wide range of operating parameters is used.

A multidiode model takes away some of these limitations by individually taking into account the subcells and connecting them in series. It has been shown that an extension from a single to a multidiode model improves the modeling accuracy at limited computational costs (which increases linearly with the number of subcells) [17]. However, just as its single-diode counterpart, multidiode models do not take into account the effects of distributed resistances.

Distributed models such as SPICE are normally used when these distributed effects need to be taken into account. In a distributed SPICE model, the cell is split up into a large number of small spatial elements. Each element has its own set of solar cell parameters such as dark current, series resistance, and ideality factor, thus allowing the model to more accurately account for variations in local current and voltage due to these spatially varying parameters. Although more accurate, using a SPICE model also enormously increases computational costs as the number of elements used is typically very large and each element is solved individually. Furthermore, in order to successfully model an MJ solar cell using a SPICE model, various fundamental parameters of the (sub)cell, most notably the resistances of all different layers, are required as an input. These data are not always readily available.

In this paper, we demonstrate that, for the optimization of concentrator MJ solar cell front contact grids, using a multidiode model provides accurate results. We validate this statement through comparison with the literature experimental results. Furthermore, we apply our model to a complex front contact optimization problem: finding efficiency and optimal operating point for front contacts with varying redirecting capability—an increasingly important scenario in lieu of the rise of novel contact technologies.

2. Computational Modeling Approach

In order to model a solar cell's efficiency under a variety of front contact layouts and operating conditions, both the optical and the electrical aspects of the cell need to be taken into account. In the algorithm presented in this paper, these two aspects are treated sequentially. Firstly, the cell's geometry and the optical operating conditions are implemented in a combined ray- and wave-optical model developed by Mcintosh and Baker-Finch [18, 19] to calculate the resulting short circuit current density, assuming ideal internal quantum efficiency (IQE = 1) in the different subcells. Mcintosh's model allows for the integration of rectangular, nonredirecting contacts and of triangular cross section, almost perfectly redirecting contacts (ETCs). The other redirection scenarios presented in this paper were obtained through an interpolation between these two extreme cases. Furthermore, the optical simulations were performed under different irradiance angles to accurately account for the irradiance angle profile under concentration in a concentrator solar module. The resulting short circuit current density in the concentrator module was obtained through the weighting of the different angles according to the concentration configuration. The short circuit current density and all other relevant electrical parameters such as metal resistivity, finger spacing, emitter sheet resistivity, and diode ideality factor are then used as an input for the electrical multidiode model, which will be explained in more detail in the next section. With this model, the open circuit voltage V_{oc} and the fill factor FF can be calculated, and by iteration, a maximum achievable efficiency can be determined for a given set of operating or design parameters. A flow diagram of this approach is shown in Figure 1.

3. Equivalent Circuit Model

The core element of the simulation method presented here is the multidiode model of a multijunction solar cell. This model takes the single-diode equivalent circuit of a solar cell as its point of departure. The single-diode circuit is presented in Figure 2(b) and consists of a series resistance R_S, accounting for resistive losses in the cell, a shunt resistance R_{Sh}, accounting for shunt pathways in the cell which in the case of high-efficiency III–V solar cells can be taken to be of infinite value, a current source I_L accounting for the light-generated current in the cell, and a diode, accounting for the behavior of the cell in the dark. The current of each diode is given by

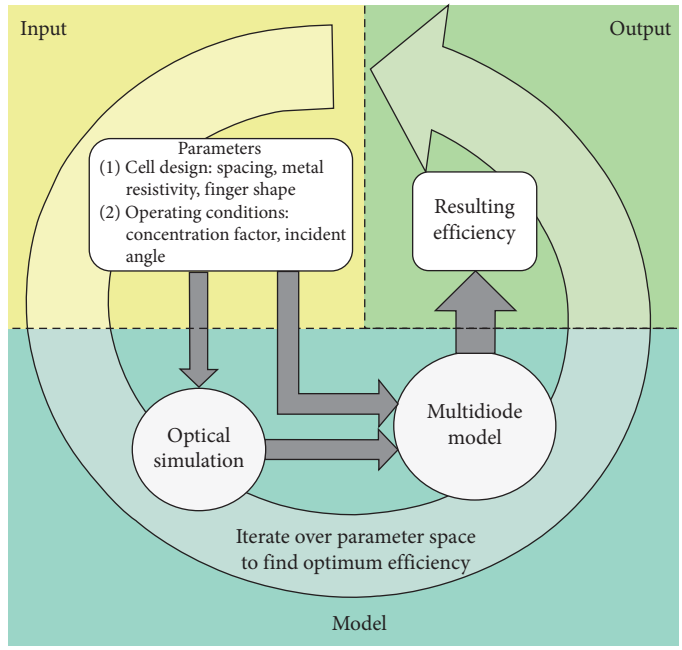

FIGURE 1: Flow diagram of the computation algorithm. First, all relevant parameters such as contact spacing and operation conditions are fed into an optical simulation. The resulting short circuit current density and additional information on the series resistance obtained from the other parameters of the cell are then used as input for the multidiode model which computes the efficiency. This process is repeated for the whole parameter space to determine optimum efficiency and operating conditions.

$$I_d = I_0\left(e^{(qV_d/mk_BT)-1}\right), \tag{1}$$

where I_d is the current through the diode, I_0 is the dark saturation current of the diode, q is the electron charge, m is the diode's ideality factor, k_B is the Boltzmann constant, T is the temperature, and V_d is the voltage across the diode.

In the multidiode model, these single diodes are connected in series by means of a tunnel diode, as is shown in Figure 2(c). Following electrical circuit theory, neglecting the −1 term in (1) and taking the shunt resistance to be infinite, it can be shown that the current-voltage relationship for each individual subcell i in Figure 2 is given by

$$I_i = I_{L,i} - I_{0,i}e^{\left(q\left(V_i - I_iR_{s,i}\right)/m_ik_BT\right)}. \tag{2}$$

These individual I–V curves can then be combined into the output I–V curve of the complete cell, which can in turn be translated into an operating efficiency.

It is worth mentioning again that the goal of the model is to calculate solar cell efficiencies for various front grid designs. The front grid influences the electrical behavior of the solar cell mainly through the series resistance (see equation (2)). In a multijunction cell, the total series resistance can be split into (1) vertical resistance through the semiconductor, (2) horizontal resistance through the top emitter layer, and (3) resistance in the electrical front grid. See Figure 2(a) for a schematic of these three sources of resistance and the layout of a typical front grid. Resistance (1) is unaffected by the front grid because it comprises the resistances vertical to the front grid such as bulk and interface resistance. These always have to be added to the resistances occurring from lateral charge transport. Resistances (2) and (3) change when the front grid changes as these describe the lateral charge transport. As one example, if the contacts are closer together, the path in the top emitter through which current has to be conducted is shorter, and hence, the resistance originating from the top emitter layer will be lower. As another example, the resistances originating from the electrical front grid become lower if the aspect ratio of the contacts is higher. Thus, in order to determine the effect of variations in front grid design, all four individual subcell resistances $R_{S,i}$ are combined into two resistances: one for vertical transport, R_{vert}, unaffected by the front grid (mostly resulting from the resistance of the tunnel diodes between the cells), and one, R_{front}, representing all losses at the top of the cell and in the grid [20]. R_{front} is then calculated for various grids by assuming a linear increase in current with location through the grid fingers and a linear increase in current with location in the top emitter between the fingers in the direction perpendicular to the fingers [21]. This results in the following equation for the front grid resistance R_{front}:

$$R_{\text{front}} = R_{\text{emit}} + R_{\text{contact}} + R_{\text{metal}}, \tag{3}$$

where R_{contact} is the contact resistance between metal and semiconductor and R_{emit} is the lumped resistance in the emitter sheet, given by [21]

$$R_{\text{emit}} = \frac{D^2}{12}\frac{R_{\text{sheet}}}{A_{\text{cell}}}, \tag{4}$$

and R_{metal} is the lumped resistance in the metal front grid, given by [21]

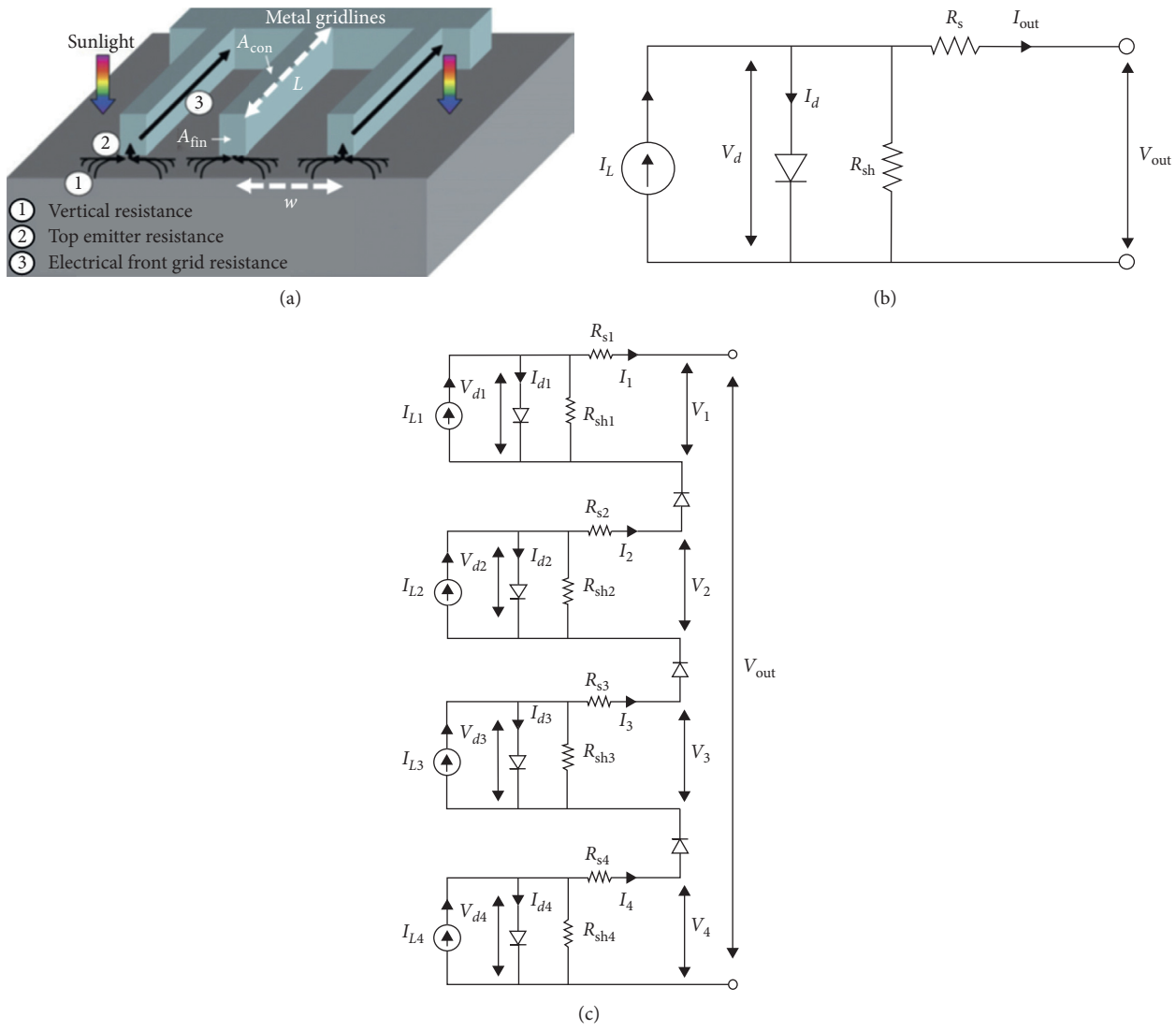

FIGURE 2: (a) Schematic overview of the current flow and layout of the front side of a multijunction solar cell. Numbers 1, 2, and 3 indicate the sources of resistance as indicated in the text, (b) the single-diode model equivalent circuit, and (c) equivalent circuit of the multidiode model.

$$R_{\text{metal}} = \frac{\rho_{\text{line}} L}{3 n_f}. \tag{5}$$

The geometry is explicitly taken into account in these equations: D is the distance between two fingers, A_{cell} the sun-facing area of the cell, L the length of the fingers, and n_f the number of perpendicular fingers. The metal line resistivity is given by ρ_{line}. See Figure 2(a) for an overview of the used geometry.

4. Comparison with Experimental Results

In order to validate the proposed model, the parameters of a state-of-the-art high-quality four-junction solar cell [22] were used as input parameters for our simulations. Concentration-dependent fill factor and I-V curves were directly obtained from reference [22] and the total series resistance was derived from the I-V curves. Electrical front grid parameters and top emitter sheet resistance were obtained through personal communication with the authors of reference [22]. In the following, our multidiode simulation results will be compared with the experimental results from this cell.

The fill factor vs. concentration curves for the multidiode model and the experimental result are shown in Figure 3. It can be seen that the multidiode model follows the experimental points closely. The most important reason for this is that the actual operating conditions and experimental data of the modeled cell can be implemented more directly into the multidiode model. For instance, for the multidiode model, the total series resistance is taken directly from the reported I-V and FF curves, whereas the series resistance in the SPICE model is calculated in a bottom-up approach. The bottom-up approach is helpful if the experimental cell parameters (such as tunnel diode resistance) are not known. In the multidiode model, one has to deduct those parameters

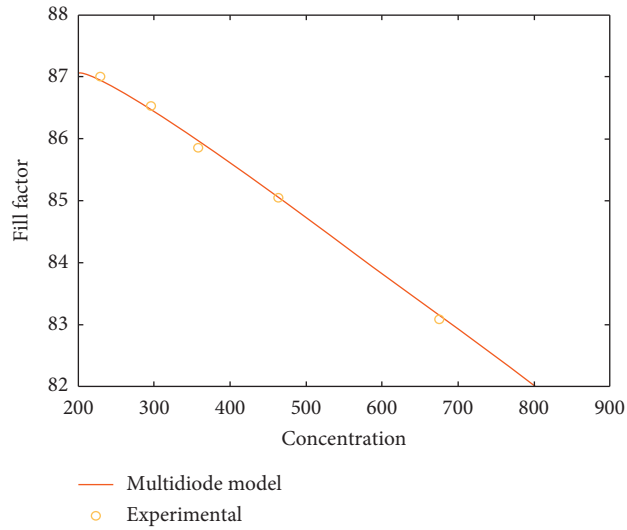

Figure 3: Comparison of FF obtained from multidiode model and experimental results taken from [22].

from relevant literature data. If the experimental behavior of the cell is already known in detail for one specific front contact configuration and these data are available, then this deduction is possible and the multidiode model is superior as those parameters can be used directly. If this is not the case however, it should be emphasized that a bottom-up approach in the form of a SPICE model remains preferable due to its more fundamental nature as explained in the literature [1].

5. Optimizing Front Grid Designs for Multijunction Cells under Concentration

Due to the efficient design of the model and the high accuracy for cases in which the experimental cell properties are well known, as described in the previous sections, it is possible to simulate multijunction cells under concentration over a large parameter space without excessive computation times. In this section, the four-junction cell as introduced earlier [22] is taken as an example of which potential efficiency improvements are calculated for various front grid designs.

First of all, the effect of varying grid density (finger periodicity) is investigated, assuming flat, 5 μm wide, completely reflecting silver fingers. This is done by changing the number of fingers in our model and calculating the resulting effect (both optical and electrical) on the solar cell's performance. Concentration factors ranging from 0 to 1000 times were used with an irradiance spectrum of air mass 1.5 global (AM1.5G). The results are shown in Figure 4. Figure 4(a) shows the concentration-dependent FF for different periodicities ranging from 48 μm to 338 μm. For low concentration, the FF slightly increases with concentration due to the increase in light-generated current relative to dark current. For high concentration, the FF decreases due to resistive losses and decreases faster for increasing finger periodicity. The decrease of both R_{emit} and R_{metal} with decreasing periodicity (see equations (4) and (5)) leads to an increase in fill factor. This effect is especially pronounced at higher concentrations as the resistive losses scale with the square of the current.

Counterworking this effect, however, is the reduction in short circuit current with decreasing periodicity as can be seen in Figure 4(b). Although, obviously, short circuit current increases linearly with concentration for all cells, it does so at a higher rate for lower periodicities due to the decrease in shading. The two competing processes shown in Figures 4(a) and 4(b) can be combined into a concentration-dependent efficiency as shown in Figure 4(c). Note that we also accounted for the minor changes in the open circuit voltages not shown in any graph.

From there, it can be seen that for each periodicity, the maximum efficiency occurs at a different concentration, with the maxima of the largest periodicities occurring at the lowest concentrations, again due to the increase in resistive power losses with the square of the current (concentration). It can also be seen that for a specific cell layout, there is an optimal spacing, which in this case is close to 169 μm, shown in purple. Larger periods lead to a rapid decline in efficiencies at higher concentrations due to resistive losses, and lower periods lead to an overall suppressed efficiency due to shading.

6. Optimizing Redirecting Front Grids

With the advent of novel high aspect ratio printing methods and contacts with sophisticated photonic design, it is informative, both from a theoretical and from a practical perspective, to look not only at flat, fully reflecting fingers but also at fingers that redirect part of the incoming light towards the active cell area. From a theoretical point of view, this allows us to develop more insight into how the shading versus resistance trade-off as seen in Figure 4 changes with changing finger design. From a practical point of view, it is important to quantify the advantage of (partially) redirecting fingers such that through technoeconomical modeling, it can

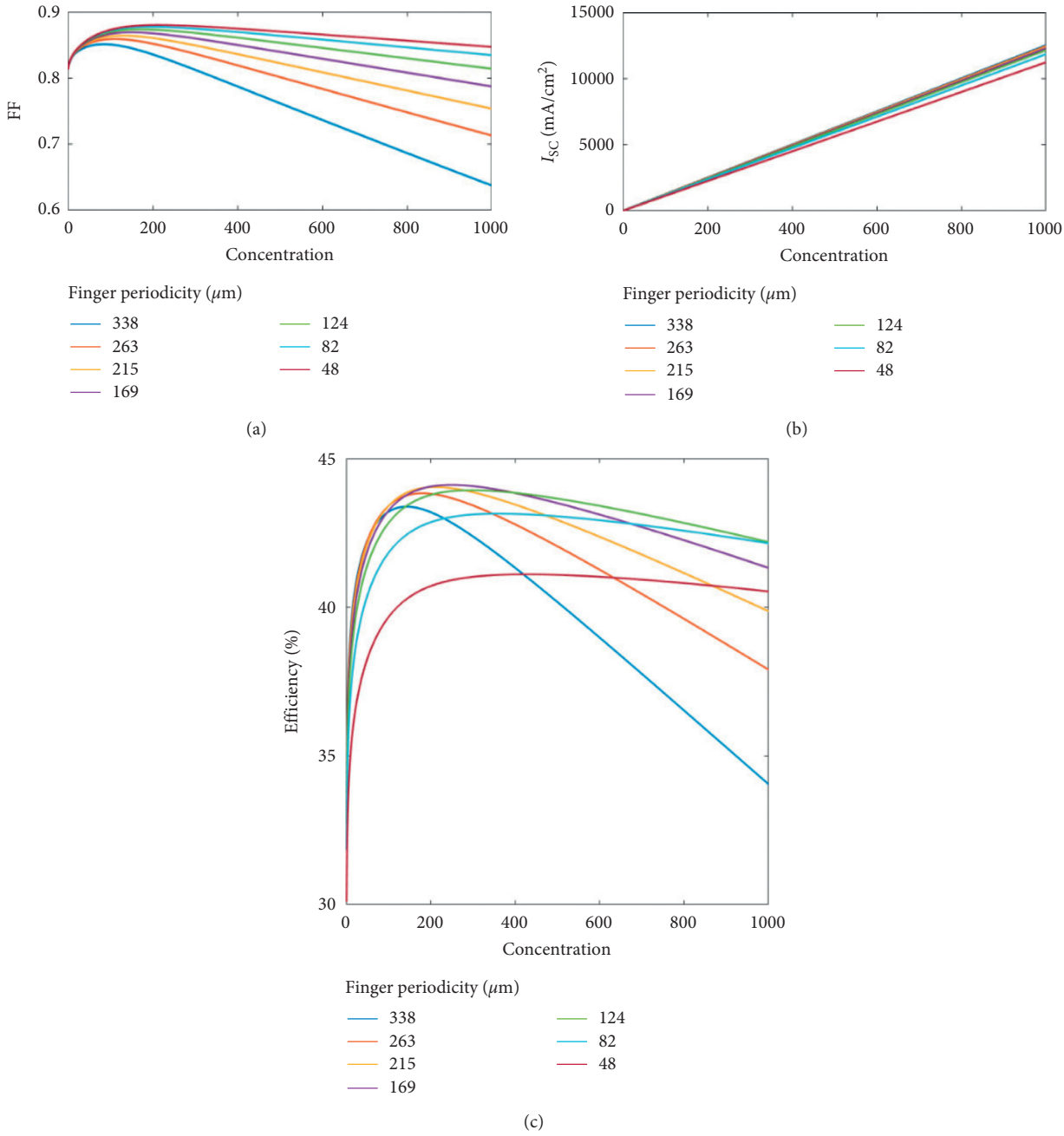

Figure 4: Fill factor, short circuit current, and the resulting efficiency for nonredirecting fingers as a function of concentration and for 5 selected periodicities.

be assessed whether the added benefits justify the enhanced fabrication complexity.

We quantify the amount of light reflected from the fingers towards the cell as the redirection capability of a finger grid, which is defined as the amount of light that is redirected towards the cell as a percentage of the total amount of light falling onto the grid fingers. 100% redirection means that all light falling onto the finger is absorbed in the cell, while 0% redirection corresponds to regular, completely reflecting fingers. Almost ideal redirection has been experimentally demonstrated [7, 8, 10, 11] and optically modeled [13, 14] only with effectively transparent contacts (ETCs) while 0% redirection occurs for completely flat and specular contacts, in which total internal reflection at the encapsulation layer can be completely neglected.

The I-V characteristics of 0%, 50%, and 100% redirecting fingers are calculated as a function of finger periodicity at a specific concentration (in this case, 300 times AM1.5). The resulting I_{sc} and V_{oc} and fill factor as a function of finger periodicity are shown in Figure 5.

Firstly, it can be seen from Figure 5(b) that the fill factor is independent of the amount of redirection. This is because the redirection parameter only affects the optical performance and does not influence the resistance and thus the

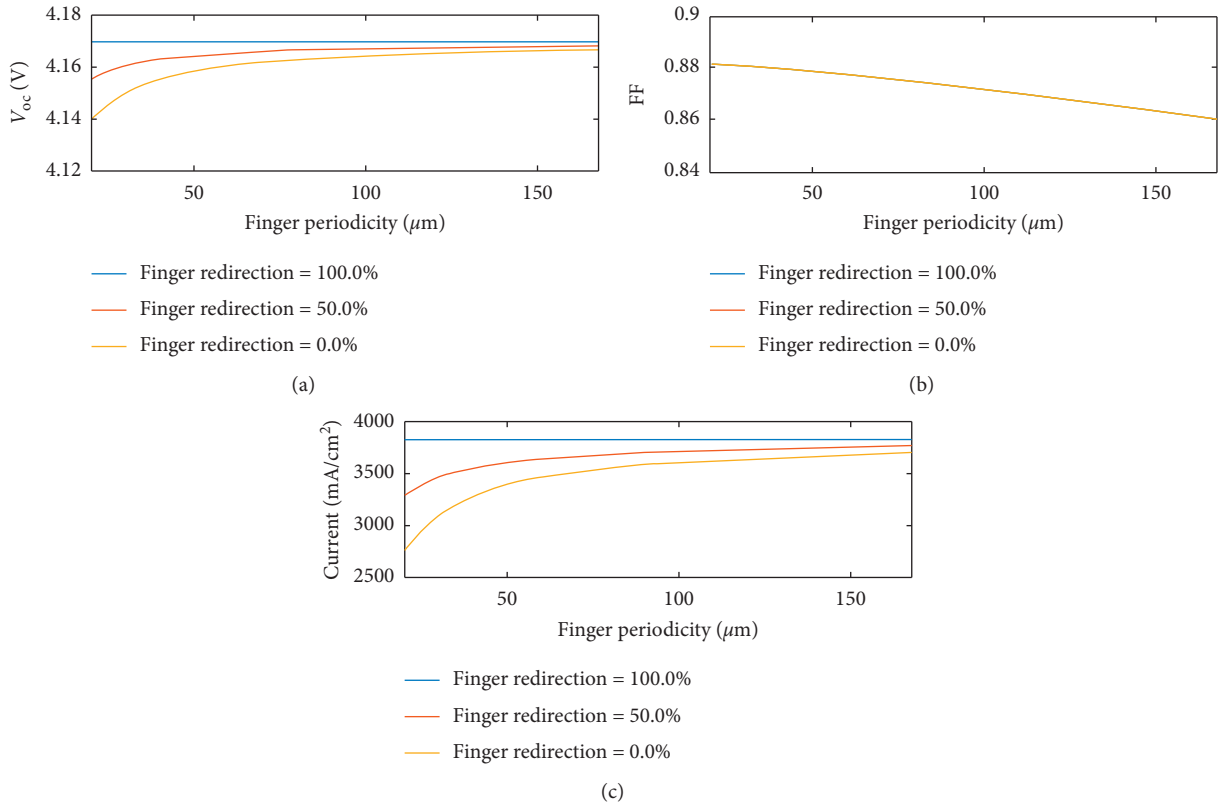

Figure 5: (a) Open circuit voltage, (b) fill factor, and (c) short circuit current density as a function of periodicity for 0%, 50%, and 100% redirection. The graph shown is simulated under 300x concentration. The decrease in current and voltage at low periodicities is strongly reduced with increasing redirection.

electrical performance. Secondly, Figures 5(a) and 5(c) show that the short circuit current and open circuit voltage are independent of the finger periodicity for completely redirecting fingers, while declining strongly with decreasing redirection and decreasing period. The nonlinear behavior along the x-axis in Figure 5(c) can be explained by considering that the generated current scales with the open cell area, which does not scale linearly with the finger period.

From Figure 5, it can be concluded that at any given finger periodicity, an increase in redirection capability always leads to an increase in generated current (and voltage), with the benefits of redirection increasing significantly with decreasing periodicity.

In order to fully utilize the model's capabilities, the combined effects of redirection, concentration, and finger periodicity can be evaluated. This allows us to determine the highest achievable efficiency for a given MJ cell if the front contact grid can be freely designed. The simulation is performed by assuming a number of finger redirection capabilities (similar to the results presented in Figure 5), calculating their period-dependent efficiency as a function of concentration (similar to the results presented in Figure 4), and determining the maximum achievable efficiency for any given combination of period and redirection (the maximum in a concentration vs. efficiency curve). These maxima can then be plotted as a function of redirection and periodicity. The results of this simulation are shown in Figure 6.

In Figure 6, a similar trend can be observed as in Figure 5, where lower periods caused a current and voltage decrease and a fill factor increase. In Figure 6, the combination of these two competing effects translates into a local maximum in the maximum achievable efficiency as a function of periodicity for a given amount of redirection. In other words, Figure 6 shows the optimal finger periodicity for a given solar cell and finger design. The optimal periodicity shifts to lower values when the fingers can redirect more light since the redirection shifts the balance between optical drawbacks and electrical benefits of a denser finger grid.

Even more importantly, it can be seen that significant efficiency gains of >1% absolute are achievable by increasing the amount of finger redirection. For instance, by changing the currently used fingers with a 36% redirection capability to effectively transparent contacts (ETCs) [7], which have a 97.7% redirection capability [10], the efficiency can be increased to 46.6%, an increase of 1.9% absolute. It can be seen that the relative efficiency increases by ~7% when replacing 0% redirecting contacts with 100% redirecting contacts and optimizing the periodicity.

It should be emphasized that the graph in Figure 6 does not only present one single concentration condition, but is composed of individual maxima taken from individual efficiency versus concentration curves. This gives a feeling for the amount of computation that is needed in order to obtain

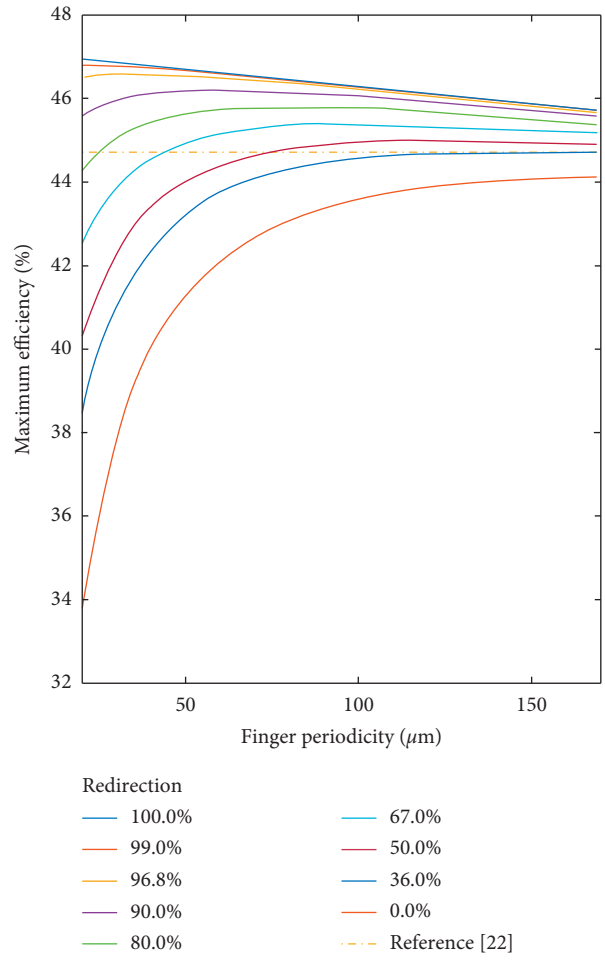

Figure 6: Maximum achievable efficiencies for various values of redirection capability, as a function of finger periodicity. It is shown that significant efficiency gains can be obtained by increasing the amount of redirection and moving to lower periodicities. The dashed yellow curve indicates the result presented in [22]. Note that the maximum efficiencies occur at higher concentrations when going to lower periodicities and higher redirecting capabilities (see Figure 7).

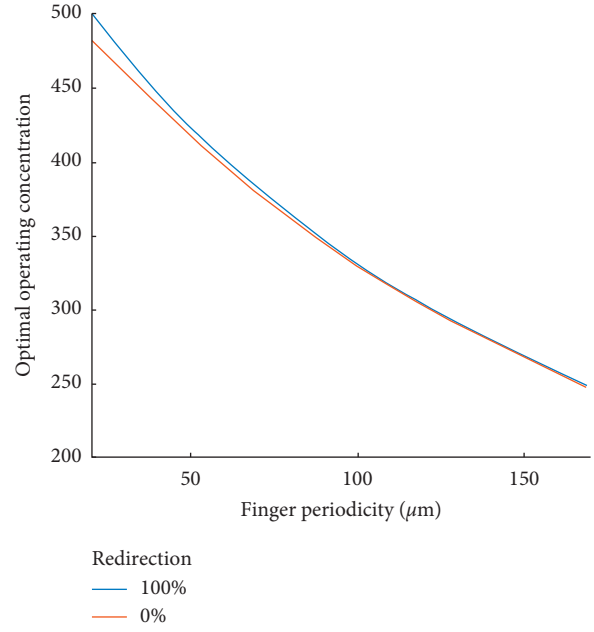

Figure 7: Concentration at which the maximum efficiencies in Figure 6 occur, as a function of finger periodicity for completely redirecting (blue curve) and completely reflecting (red curve) fingers.

this graph and thus the benefits of using the efficient multidiode approach presented in this paper. Furthermore, it follows that the optimal operating concentration changes with both finger periodicity and amount of redirection. The optimal concentration at which maximum efficiency occurs dependent on the finger periodicity is shown in Figure 7 for nonredirecting (0%) and perfectly redirecting (100%) contacts. It can be seen that generally, to achieve the higher efficiencies at lower periodicities, higher operating concentrations are necessary. The difference between strongly and weakly redirecting fingers however is rather small and only becomes pronounced with small finger periodicity. This shows that a once-determined optimal concentration will stay somewhat constant for enhanced contact redirection capability and is not the most crucial parameter to optimize.

7. Conclusion

In summary, we have shown that a multidiode model fed with optical absorption modeling results and experimental solar cell parameters offers an accurate and computationally efficient way to optimize front contact grids in concentrator multijunction solar cells. The multidiode model accurately describes the experimental properties of the solar cell if the solar cell parameters are known for a specific front contact design. The SPICE model is only superior if those experimental parameters are unknown. On the other hand, the multidiode model is superior if detailed knowledge on the interface resistance is unavailable, but the solar cell parameters are known. We have applied our multidiode model to the optimization of front contact grids with different redirection capabilities. We found that the maximum achievable efficiency can be enhanced by ~7% relative if 0% redirecting contacts are replaced by 100% redirecting contacts. The presented model will facilitate the design of optimized front contact layouts in an area of emerging, high-performance front contact technologies.

Data Availability

The computational data used to support the findings of the study are available within the article.

Conflicts of Interest

The authors declare no conflicts of interest.

Acknowledgments

The authors would like to thank Mark Steiner, Eduard Oliva, and Frank Dimroth (all from Fraunhofer ISE) for fruitful discussion and support.

References

[1] M. Steiner, S. P. Philipps, M. Hermle, A. W. Bett, and F. Dimroth, "Validated front contact grid simulation for GaAs solar cells under concentrated sunlight," *Progress in Photovoltaics: Research and Applications*, vol. 19, no. 1, pp. 73–83, 2011.

[2] C. Honsberg and S. Bowden, 2020, https://www.pveducation.org/pvcdrom/design-of-silicon-cells/optimization-of-finger-spacing.

[3] L. Nagel and D. Pederson, "Simulation program with integrated circuit emphasis," in *Proceedings of the Midwest Symposium on Circuit Theory*, University of Illinois at Urbana-Champaign, Champaign, IL, USA, 1973.

[4] P. Espinet-González, R. Mohedano, I. García et al., "Triple-junction solar cell performance under Fresnel-based concentrators taking into account chromatic aberration and off-axis operation," in *Proceedings of the AIP Conference Proceedings*, pp. 81–84, Kuala Lumpur, Malaysia, June 2012.

[5] P. Kuang, J.-M. Park, W. Leung et al., "A new architecture for transparent electrodes: relieving the trade-off between electrical conductivity and optical transmittance," *Advanced Materials*, vol. 23, no. 21, pp. 2469–2473, 2011.

[6] J. S. Ward, A. Duda, D. J. Friedman, J. Geisz, W. McMahon, and M. Young, "High aspect ratio electrodeposited Ni/Au contacts for GaAs-based III–V concentrator solar cells," *Progress in Photovoltaics: Research and Applications*, vol. 23, no. 5, pp. 646–653, 2015.

[7] R. Saive, A. M. Borsuk, H. S. Emmer et al., "Effectively transparent front contacts for optoelectronic devices," *Advanced Optical Materials*, vol. 4, no. 10, pp. 1470–1474, 2016.

[8] R. Saive, C. R. Bukowsky, S. Yalamanchili et al., "Effectively transparent contacts (ETCs) for solar cells," in *Proceedings of the 2016 IEEE 43rd Photovoltaic Specialists Conference (PVSC)*, pp. 3612–3615, Portland, OR, USA, June 2016.

[9] H. A. Atwater, R. Saive, A. M. Borsuk, H. Emmer, C. Bukowsky, and S. Yalamanchili, "Solar cells and methods of manufacturing solar cells incorporating effectively transparent 3D contacts," Google Patents, 2016.

[10] R. Saive, M. Boccard, T. Saenz et al., "Silicon heterojunction solar cells with effectively transparent front contacts," *Sustainable Energy & Fuels*, vol. 1, no. 3, pp. 593–598, 2017.

[11] R. Saive, S. Coplin, H. L. Kim, Chris H. Van de Stadt, M. D. Kelzenberg, and H. A. Atwater, "Transparent, conductive and lightweight superstrates for perovskite solar cells and modules," in *Proceedings of the 2018 IEEE 7th World Conference on Photovoltaic Energy Conversion (WCPEC) (A Joint Conference of 45th IEEE PVSC, 28th PVSEC & 34th EU PVSEC)*, Waikoloa Village, HI, USA, June 2018.

[12] P. G. Kik, "Catoptric electrodes: transparent metal electrodes using shaped surfaces," *Optics Letters*, vol. 39, no. 17, pp. 5114–5117, 2014.

[13] R. Saive and H. A. Atwater, "Mesoscale trumps nanoscale: metallic mesoscale contact morphology for improved light trapping, optical absorption and grid conductance in silicon solar cells," *Optics Express*, vol. 26, no. 6, pp. A275–A282, 2018.

[14] R. Saive, T. C. R. Russell, and H. A. Atwater, "Enhancing the power output of bifacial solar modules by applying effectively transparent contacts (ETCs) with light trapping," *IEEE Journal of Photovoltaics*, vol. 8, no. 5, pp. 1183–1189, 2018.

[15] G. S. Kinsey, P. Hebert, K. E. Barbour, D. D. Krut, H. L. Cotal, and R. A. Sherif, "Concentrator multijunction solar cell characteristics under variable intensity and temperature," *Progress in Photovoltaics: Research and Applications*, vol. 16, no. 6, pp. 503–508, 2008.

[16] A. B. Or and J. Appelbaum, "Dependence of multi-junction solar cells parameters on concentration and temperature," *Solar Energy Materials and Solar Cells*, vol. 130, pp. 234–240, 2014.

[17] E. F. Fernández, A. J. García-Loureiro, and G. P. Smestad, "Multijunction concentrator solar cells: analysis and fundamentals," in *High Concentrator Photovoltaics*, pp. 9–37, Springer, Berlin, Germany, 2015.

[18] K. R. McIntosh and S. C. Baker-Finch, "OPAL 2: rapid optical simulation of silicon solar cells," in *Proceedings of the 2012 38th IEEE Photovoltaic Specialists Conference (PVSC)*, pp. 265–271, Austin, TX, USA, June 2012.

[19] K. R. McIntosh, 2018, https://www.pvlighthouse.com.au/sunsolve.

[20] M. Steiner, W. Guter, G. Peharz, S. P. Philipps, F. Dimroth, and A. W. Bett, "A validated SPICE network simulation study on improving tunnel diodes by introducing lateral conduction layers," *Progress in Photovoltaics: Research and Applications*, vol. 20, no. 3, pp. 274–283, 2012.

[21] A. R. Burgers, *New metallisation patterns and analysis of light trapping for silicon solar cells*, Ph.D. thesis, Energieonderzoek Centrum Nederland, Sint Maartensvlotbrug, Netherlands, 2005.

[22] F. Dimroth, M. Grave, P. Beutel et al., "Wafer bonded four-junction GaInP/GaAs//GaInAsP/GaInAs concentrator solar cells with 44.7% efficiency," *Progress in Photovoltaics: Research and Applications*, vol. 22, no. 3, pp. 277–282, 2014.